Journal of
Materials Chemistry A

PAPER

View Article Online
View Journal | View Issue

Check for updates

Cite this: *J. Mater. Chem. A*, 2019, **7**, 23941

Structural engineering to maintain the superior capacitance of molybdenum oxides at ultrahigh mass loadings†

Ji-Chi Liu,[a] Hui Li,[a] Munkhbayar Batmunkh,[b] Xue Xiao,[c] Ying Sun,[a] Qin Zhao,[a] Xue Liu,[a] Zi-Hang Huang *[a] and Tian-Yi Ma *[c]

Capacitance loss with the increase of mass loading, originating from the slow electron and ion migration kinetics through the thick electrode materials, has been the subject of intense investigation in the field of supercapacitors. In this work, we report the preparation of a mixed-valence molybdenum oxide (MoO_{3-x}) electrode with an ultrahigh mass loading of 15.4 mg cm^{-2} on a functionalized partially exfoliated graphite substrate using a facile electrochemical method. In addition to the highly open graphene nanosheets atop, the unique layered structures of intercalated graphite sheets ensure efficient ionic transport in the entire MoO_{3-x} electrode. The oxygen-containing functional groups on the exfoliated graphene can bind strongly with the MoO_{3-x} *via* formation of C–O–Mo bonding, which provides a fast electron transport path from graphene to MoO_{3-x} and thus allows high reversible capacity and excellent rate performance. The optimized MoO_{3-x} electrode delivers an outstanding areal capacitance of 4.03 F cm^{-2} at 3 mA cm^{-2} with an excellent rate capability which is significantly higher than the values of other molybdenum oxide based electrodes reported to date. More importantly, the areal capacitance increases proportionally with the MoO_{3-x} mass loading, indicating that the capacitive performance is not limited by ion diffusion even at such a high mass loading. An asymmetric supercapacitor (ASC) assembled with an MoO_{3-x} anode delivers a maximum volumetric energy density of 2.20 mW h cm^{-3} at a volumetric power density of 3.60 mW cm^{-3}, which is superior to those of the majority of the state-of-the-art supercapacitors.

Received 9th May 2019
Accepted 8th July 2019

DOI: 10.1039/c9ta04835a

rsc.li/materials-a

Introduction

The rapid development of portable and wearable electronic devices has stimulated ever-growing interest in the exploration of high-efficiency electrochemical energy storage devices. With the excellent features of balancing the need of high energy density and fast charging/discharging, pseudocapacitors have been considered as emerging high-efficiency energy storage devices, demonstrating great promise in the market.[1–4] Among various pseudocapacitive materials, molybdenum oxide (MoO_3) has attracted a great deal of attention owing to its high theoretical capacitance, multiple stable oxidation states, and environmentally friendly nature.[5,6] However, although achieving good specific capacitance, the reported MoO_3 materials exhibited relatively small mass loadings of active materials (0.3–1.8 mg cm^{-2}).[7–10] The total capacitance and energy stored in such low mass loading materials are, in fact, considered very low, which substantially limits their practical feasibility for high energy systems.[11] It should be noted that the commercially available electrodes usually require a typical mass loading of about 8–10 mg cm^{-2} for the active materials.[12–14] However, increasing MoO_3 loading or film thickness often causes severe deterioration of capacitive performance (rate capability and specific capacitance) due to inefficient ion diffusion and electron transport.[5,11] Therefore, improving the rate capability and specific capacitance of highly loaded MoO_3 electrodes, especially at high current density, is of great urgency to satisfy the requirements of high-efficiency electrochemical energy storage systems.

The reasons for the capacitance deterioration of highly loaded MoO_3 electrodes can be two-fold. The slow ion diffusion in a densely packed and thick film is problematic when the mass loading of MoO_3 is high. Likewise, the electron transport is also expected to be hindered in a thick, nonconductive MoO_3 film. A feasible strategy to enhance the rate capability of high mass loading materials is to deposit active species onto three-dimensional (3D) and high-surface-area substrates (current

---

[a] *Institute of Clean Energy Chemistry, Key Laboratory for Green Synthesis and Preparative Chemistry of Advanced Materials, College of Chemistry, Liaoning University, Shenyang 110036, China. E-mail: huangzihang@lnu.edu.cn*

[b] *Australian Institute for Bioengineering and Nanotechnology, University of Queensland, St. Lucia, QLD, 4072 Australia*

[c] *Discipline of Chemistry, University of Newcastle, Callaghan, NSW 2308, Australia. E-mail: Tianyi.Ma@newcastle.edu.au*

† Electronic supplementary information (ESI) available. See DOI: 10.1039/c9ta04835a

collectors), resulting in the formation of conductive linkages between active materials and substrates.[11,13] This can effectively improve both the mass and charge transport in the electrodes. For example, Ji *et al.* designed and prepared a sandwiched MoO_3/C nanostructure which delivered an outstanding energy storage performance due to the high degree of graphitization in the graphene layer and more interlayered void regions.[5] MoO_3 assembled on the 3D layered structure of graphene oxide frameworks *via* oxygen-bonding interactions at the interface was also reported to show improved electrochemical performance due to the rapid ion diffusion and electron transport of 3D graphene frameworks.[15] Zhou and co-workers reported metal–O–C bonds between metal oxide and carbonaceous materials incorporating oxygen functional groups based on first-principles calculations.[16] They found that NiO was bonded strongly to graphene through oxygen bridges, which facilitated electron hopping from graphene to NiO and thus allowed high reversible capacity and excellent rate performance. Despite some limitations such as limited total capacitance and mass loading, this work has been successfully demonstrated to effectively address the slow ion diffusion and electron transport in highly loaded molybdenum oxide electrodes which would help to realize high energy storage capacity without sacrificing their electrochemical performance. Therefore, designing and engineering highly loaded molybdenum oxide electrodes that can provide rapid ion diffusion and charge transport, while exhibiting excellent specific capacitance and rate capability, is of great interest.

Herein, a unique mixed-valence molybdenum oxide (MoO_{3-x}) with an ultrahigh mass loading of up to 15.4 mg cm^{-2} on functionalized partially exfoliated graphite (FEG) is designed for pseudocapacitors. The prepared electrode exhibits efficient ionic and electric transport due to the unique layered structures and highly open graphene sheets atop. The MoO_{3-x} electrode achieves an outstanding areal capacitance of 4.34 F cm^{-2} at 1 mA cm^{-2} and excellent rate capability. Finally, the asymmetric supercapacitor (ASC) assembled with our MoO_{3-x} anode exhibits an extremely high volumetric energy density of 2.20 mW h cm^{-3}, superior to those of most state-of-the-art supercapacitors.

Results and discussion

Electrode characterization

The functionalized partially exfoliated graphite (FEG) substrate was prepared by the electrochemical exfoliation method that was modified on the basis of our previous work.[17] As shown in Fig. 1a, the side view scanning electron microscopy (SEM) image reveals that the substrate is constructed from multiple exfoliated graphite layers which are seamlessly connected to each other. The FEG consists of a top layer of partially exfoliated graphene sheets (Fig. S1b†) and a bottom layer of expanded graphite layers (Fig. S1c†). This provides a large amount of void space and macroporous structure which will allow facile ion intercalation/de-intercalation into the electrode interior. The top view SEM images in Fig. S1d and e† reveal the interconnected macroporous architecture of the FEG substrate. From the TEM image in Fig. S1f,† it can be seen that the exfoliated graphene sheets have good crystallinity with thickness at the nanometer scale. Moreover, the functional groups (oxygen-containing groups) on the surface provide a strong interaction with various nucleation sites for the deposited metal oxides, thus ensuring the homogenous growth of the latter, which is expected to facilitate electron hopping from the graphene to metal oxide.[16]

The MoO_{3-x} was then electrodeposited onto the FEG substrate with a mass loading of 15.4 mg cm^{-2} using a potentiostatic process. As shown in Fig. 1b, the porous exfoliated graphite layers are coated with MoO_{3-x}, maintaining the layered structure despite being largely thickened. The homogeneous distribution of Mo and O, confirmed by the energy dispersive X-ray spectroscopy (EDS) mapping (Fig. 1c), demonstrates the uniform deposition of MoO_{3-x} on the FEG. We also collected the EDS spectra of the as-obtained FEG/MoO_{3-x} sample. The signal of element C is obvious, indicating that the composite is successfully fabricated (Fig. S2†). The successful fabrication of the composites indicates that the exfoliated graphite layer provides facile ionic and electric transport during the electrodeposition process. A crumpled graphene nanosheet and MoO_{3-x} can be clearly seen from the transmission electron microscopy (TEM) image of the ultrasonicated sample, confirming the successful integration of 3D graphene nanosheets and pseudocapacitive MoO_{3-x} (Fig. 1d). It is clear that no lattice fringe is observed from the high-resolution TEM images shown in Fig. S3a and b,† suggesting the amorphous nature of FEG/MoO_{3-x}. Furthermore, the amorphous nature of FEG/MoO_{3-x} is also confirmed by the SAED pattern, in which only diffusive rings can be observed (Fig. S3c†). To understand the role of the layered 3D partially exfoliated graphite in the electrode performance, we conducted further comparison among the FEG and other widely used carbonaceous substrates, including graphite foil and carbon cloth denoted as G/MoO_{3-x} and CC/MoO_{3-x}, respectively (Fig. 1e and S4†). In contrast, for the bulk graphite foil (Fig. S5a†), the majority of the MoO_{3-x} materials are deposited only on the exterior surface due to the mass transport-limited ion diffusion (Fig. S5b and d†). Besides the distinct morphologies, G/MoO_{3-x} and CC/MoO_{3-x} show apparent peeling off of the deposited species from the substrate after washing with deionized water (Fig. S5 and S6†). This peeling off was likely to start from the cracks that exist in the as-deposited electrodes, leading to their poor mechanical stability. Taken together, these results confirm the robust coupling of the FEG and pseudocapacitive MoO_{3-x}, highlighting the importance of multiple exfoliated graphite layers as a scaffold to obtain a uniform and stable coating of MoO_{3-x} at a high mass loading, determined to be 15.4 mg cm^{-2}.

The crystal structure of the electrodeposited MoO_{3-x} was characterized by X-ray diffraction (XRD, Fig. 1f). The result reveals that the deposited molybdenum oxide is amorphous in nature, possibly beneficial to the charge storage process due to the disorder and flexibility.[18] The MoO_{3-x} electrodes were also studied by X-ray photoelectron spectroscopy (XPS). For the substrates, the XPS survey spectrum of FEG exhibits an enhanced O 1s signal relative to that of G and CC (Fig. S7a†).

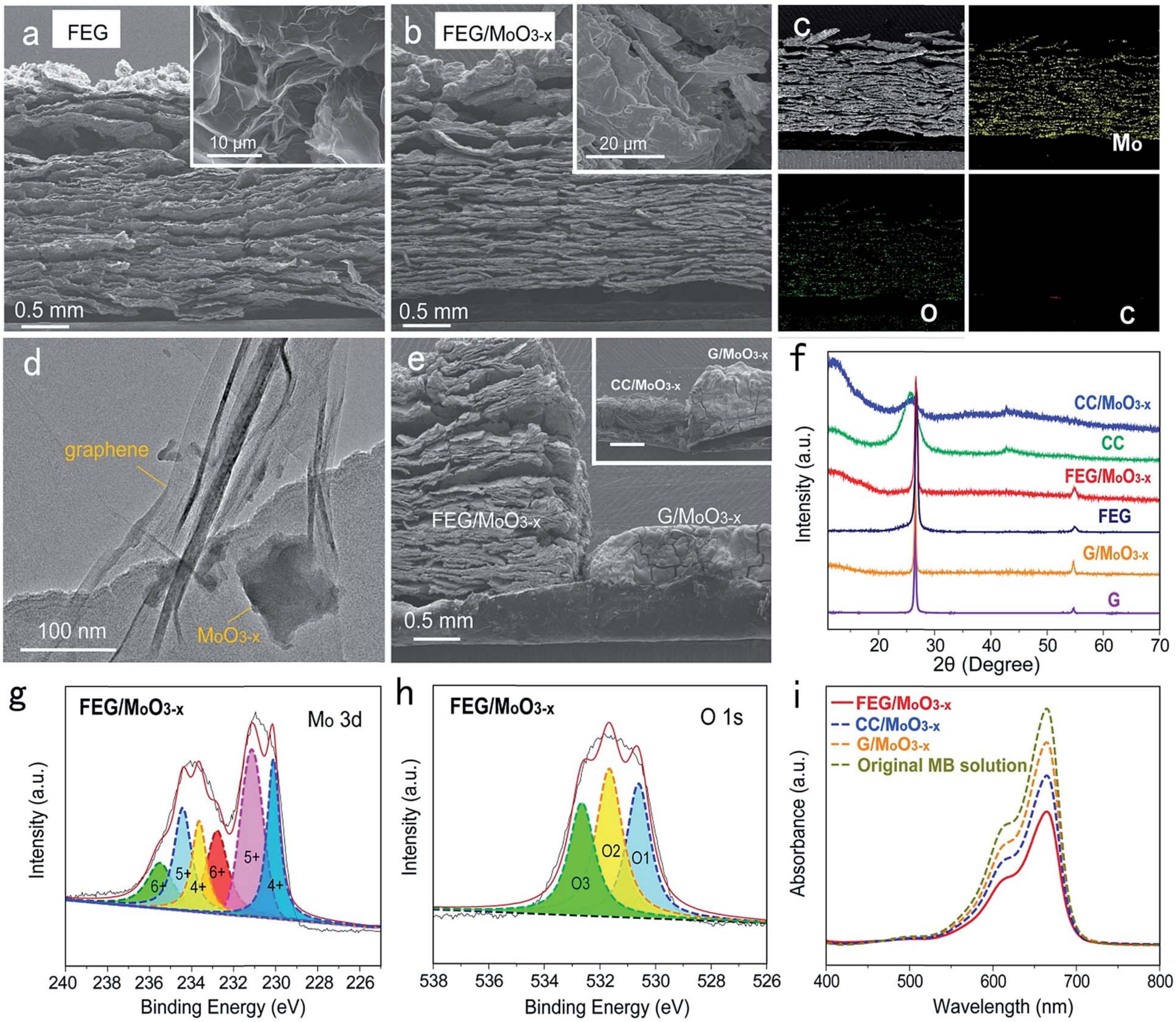

Fig. 1 Side view SEM images of (a) FEG and (b) FEG/MoO_{3-x}, insets show the top view images of these samples. (c) Elemental mapping (Mo $K_{\alpha1}$, O $K_{\alpha1}$ and C $K_{\alpha1}$) images of FEG/MoO_{3-x}. (d) TEM image of FEG/MoO_{3-x}. (e) Side view SEM images of FEG/MoO_{3-x}, G/MoO_{3-x} and CC/MoO_{3-x}. (f) XRD patterns of the as-prepared electrodes. XPS spectra of (g) Mo 3d and (h) O 1s of FEG/MoO_{3-x}. (i) UV-vis spectra collected for the original MB solution (8 mg L^{-1} in water) and the MB solutions after reaction with FEG/MoO_{3-x}, CC/MoO_{3-x} and G/MoO_{3-x} for 24 h in the dark.

The C 1s core level spectra also confirm that the FEG has a broader and higher signal than that of the G and CC substrates (Fig. S7b–d†), suggesting the existence of oxygen-containing functional groups which provide a strong interaction with the deposited metal oxides *via* metal–O–C bonding.[16] Mo 3d and O 1s core levels of the FEG/MoO_{3-x} are shown in Fig. 1g and h, respectively. In the Mo 3d spectrum, two fitted peaks at 232.9 and 235.6 eV are attributed to the $3d_{5/2}$ and $3d_{3/2}$ of Mo^{6+}, respectively. The fitted peaks at 231.3 and 234.5 eV correspond to the $3d_{5/2}$ and $3d_{3/2}$ of Mo^{5+}, while two fitted peaks at 230.1 and 233.7 eV correspond to the $3d_{5/2}$ and $3d_{3/2}$ of Mo^{4+}, respectively.[5,10,19] The O 1s peak can be deconvoluted into three components (Fig. 1h and S10†). The O1 peak at 530.6 eV is assigned to the O^{2-}; the O2 peak at 531.6 eV can be ascribed to the oxygen from the defect sites with a low oxygen coordination in the material;[20,21] the O3 peak at 532.6 eV can be assigned to the physically adsorbed and chemically bonded water or O–H.[20,22,23] The methylene blue (MB) adsorption experiments were further carried out to explore the surface area of the MoO_{3-x}-based electrodes. UV-vis absorption spectra were collected for the original MB solution and those adsorbed by FEG/MoO_{3-x}, G/MoO_{3-x} and CC/MoO_{3-x} for 24 h under dark conditions (Fig. 1i). The intensity of the characteristic absorption peak of MB (665 nm) decreases more for the FEG/MoO_{3-x} than that for the G/MoO_{3-x} and CC/MoO_{3-x}. This strong adsorption of MB dye molecules for the FEG/MoO_{3-x} is due to the larger ion accessible surface area as compared to the other samples.

Electrochemical evaluation

Electrochemical tests were performed in a three-electrode cell containing 3 M KCl as the electrolyte, saturated calomel electrode (SCE) as the reference and graphite foil as the counter electrode. A number of control experiments were performed to understand the role of the three-dimensional porous graphene architecture in the electrode performance. Fig. 2a compares the cyclic voltammograms (CVs) of the MoO_{3-x}-based electrodes that were electrodeposited on different carbonaceous substrates. Under the same loading of MoO_{3-x} (15.4 mg cm^{-2}), the CV curve of FEG/MoO_{3-x} presents a larger increase of current densities in the whole potential region compared to CC/MoO_{3-x} and G/MoO_{3-x}, demonstrating its high capacitive nature of charge storage. More importantly, the FEG/MoO_{3-x} electrode shows 67 times larger current density than the G/MoO_{3-x} electrode, revealing the substantially enhanced charge storage capability of FEG/MoO_{3-x}. This increased current for the FEG/MoO_{3-x} can be attributed to the fact that the exfoliated graphite layers are seamlessly connected with the bulky domains and form abundant void space, which enables highly efficient charge transfer and ion diffusion in this high loading electrode. Similar results were observed in the galvanostatic charge–discharge (GCD) experiments (Fig. 2b). The much longer discharge time of the FEG/MoO_{3-x} electrode further confirms its superior capacitive performance to that of the others. Fig. S11† shows the GCD profiles of the three MoO_{3-x} electrodes collected at current densities varying from 1 and 20 mA cm^{-2} (0.06–1.3 A g^{-1}). The calculated areal capacitances and gravimetric capacitances are illustrated in Fig. 2c and d. The FEG/MoO_{3-x} electrode achieves a high areal capacitance of 4.34 F cm^{-2} at a current density of 1 mA cm^{-2} (equivalent to a gravimetric capacitance of 282 F g^{-1} normalized to a mass loading of 15.4 mg cm^{-2}), which is 40 and 2 times higher than that of the G/MoO_{3-x} (0.109 F cm^{-2}, 7.1 F g^{-1}) and CC/MoO_{3-x}

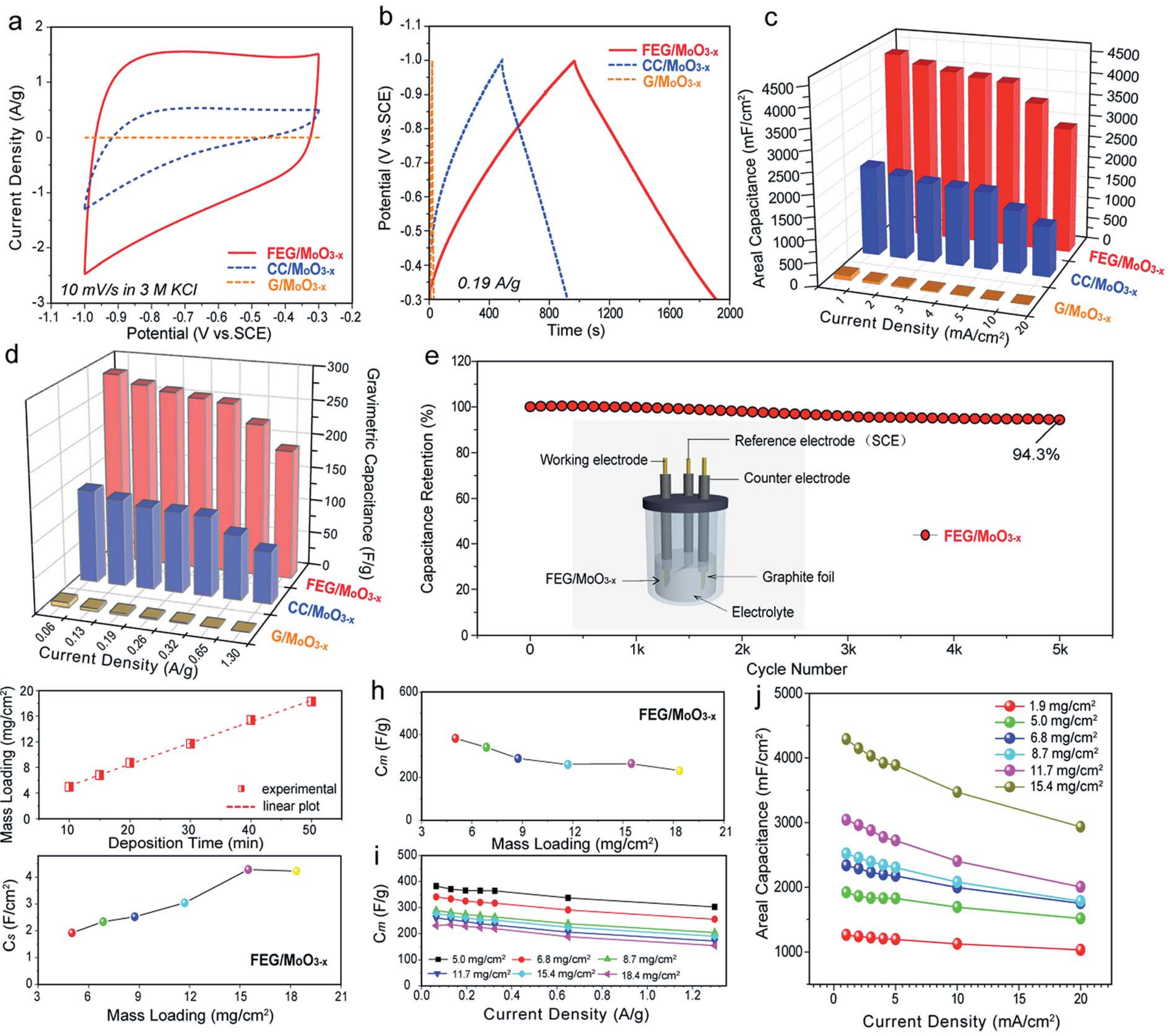

Fig. 2 Electrochemistry of the three MoO_{3-x}-based electrodes: (a) CV curves measured at a scan rate of 10 mV s^{-1}; (b) GCD profiles measured at 0.19 A g^{-1}; (c) areal capacities of the three MoO_{3-x}-based electrodes at various current densities; (d) gravimetric capacities of the three MoO_{3-x}-based electrodes at various current densities; (e) a plot of capacitance retention of FEG/MoO_{3-x} as a function of cycle number, inset shows the schematic illustration of the three-electrode cell used in this work for the electrochemical measurements; (f) relationship between the mass loading of MoO_{3-x} and the electrodeposition time; (g) areal and (h) gravimetric capacitances obtained from the FEG/MoO_{3-x} electrode with different mass loadings of MoO_{3-x}; (i) gravimetric and (j) areal capacitances obtained at different current densities from FEG/MoO_{3-x} electrodes loaded with different amounts of MoO_{3-x}.

(2.10 F cm^{-2}, 136 F g^{-1}), respectively. More importantly, under such an ultrahigh mass loading, the FEG/MoO$_{3-x}$ electrode retains an extraordinary rate capability of 67.8% from 1 to 20 mA cm^{-2} (0.06–1.3 A g^{-1}). These results clearly show the highly efficient charge transfer and ion diffusion of the FEG/MoO$_{3-x}$. In contrast, the capacitances of the other two samples decrease faster with elevated current density, retaining only 55.7% (1.17 F cm^{-2} and 76 F g^{-1} for the CC/MoO$_{3-x}$), and 1.8% (2 mF cm^{-2} and 0.13 F g^{-1} for the G/MoO$_{3-x}$) areal/gravimetric capacitance. Similar results were also obtained by CV measurements with scan rates normalized with the total charge–discharge time of the GCD processes (Fig. S12†). For example, the capacitance is calculated to be 4.40 F cm^{-2} for the FEG/MoO$_{3-x}$ electrode based on the data measured at a 0.3 mV s^{-1} scan rate, close to the 4.34 F cm^{-2} capacitance measured by GCD at the current density of 1 mA cm^{-2}, both with similar discharging time. Moreover, the FEG/MoO$_{3-x}$ electrode also exhibits excellent cycling stability with 94.3% retention of its initial capacitance after 5000 cycles (Fig. 2e).

To gain insight into the optimized mass loading and the relationship between mass loading and enhanced electrochemical performance, electrochemical tests of MoO$_{3-x}$ electrodes were conducted at different electrodeposition times (10, 15, 20, 30, 40 and 50 min). Fig. 2f shows the mass loading of the FEG/MoO$_{3-x}$ electrodes collected at different electrodeposition times, exhibiting a linear relationship of mass loading *versus* electrodeposition time for the MoO$_{3-x}$, which allows precise control of MoO$_{3-x}$ loading. The areal capacitance of FEG/MoO$_{3-x}$ electrodes is also proven to be proportional to the MoO$_{3-x}$ loading, peaking at 4.34 F cm^{-2} at a deposition time of 40 min, followed by a slight decrease at 50 min deposition (Fig. 2g). This result indicates that the ion diffusion limits the capacitive performance at an ultrahigh mass loading of 18.4 mg cm^{-2} obtained after 50 min deposition. The FEG/MoO$_{3-x}$ electrode shows high capacitance retention with increasing the mass loading from 5 to 15.4 mg cm^{-2} (Fig. 2h). The gravimetric capacitance of the FEG/MoO$_{3-x}$ electrode decreases by only 26% from 382 to 282 F g^{-1} at 0.06 A g^{-1} when the mass loading increases from 5 to 15.4 mg cm^{-2}. The GCD profiles of FEG/MoO$_{3-x}$ electrodes with different mass loadings are shown in Fig. S13–S16† collected at different current densities. The calculated gravimetric and capacitances collected at current densities are illustrated in Fig. 2i and j. It is worth mentioning that under different mass loadings (5–15.4 mg cm^{-2}), all FEG/MoO$_{3-x}$ electrodes retain outstanding rate capabilities of 79–67.8% from 1 to 20 mA cm^{-2} (or 0.06–1.3 A g^{-1}), which are the highest values reported for the MoO$_3$-based electrodes (Table S1†). Besides, our FEG/MoO$_{3-x}$ electrode also displays excellent electrochemical performance within the potential window of 0 to 0.8 V in 0.5 M H$_2$SO$_4$ electrolyte (Fig. S17†). The FEG/MoO$_{3-x}$ electrode achieves a high areal capacitance of 1.91 F cm^{-2} at a current density of 1 mA cm^{-2} and exhibits excellent

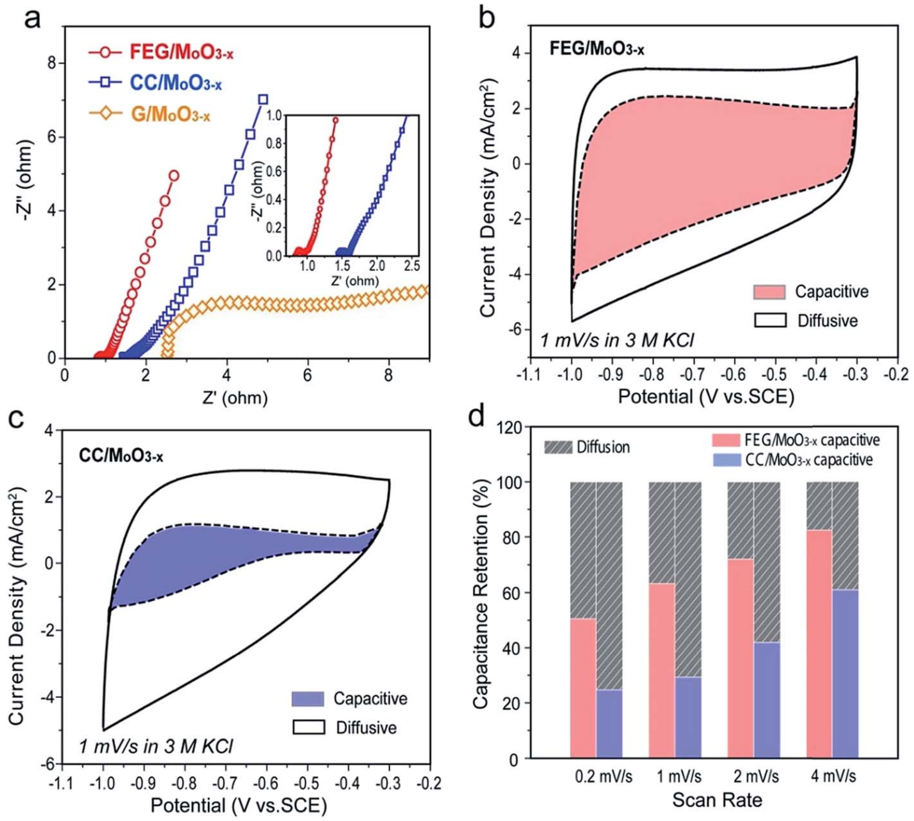

Fig. 3 (a) Nyquist plots and high frequency domain of the three MoO$_{3-x}$-based electrodes collected at open circuit potential with a perturbation of 10 mV. Capacitance separation analysis results of (b) FEG/MoO$_{3-x}$ and (c) CC/MoO$_{3-x}$ at the scan rate of 1 mV s^{-1}. (d) Normalized contribution ratio of capacitances at different scan rates of FEG/MoO$_{3-x}$ and CC/MoO$_{3-x}$.

rate capability. When the current density increases from 1 to 20 mA cm^{-2}, the FEG/MoO$_{3-x}$ retains 90.3% of its initial capacitance, demonstrating a considerably high areal capacitance of 1.72 F cm^{-2} at high current density. Overall, the aforementioned results demonstrate the outstanding energy storage capacity of the FEG/MoO$_{3-x}$ for pseudocapacitors.

Discussion

Electrochemical impedance spectroscopy (EIS) was further utilized to explore the electrochemical performance of our FEG/MoO$_{3-x}$. As shown in Fig. 3a, the FEG/MoO$_{3-x}$ presents a considerably steeper slope in the middle- and low-frequency domains as compared to the G/MoO$_{3-x}$ and CC/MoO$_{3-x}$, indicating that the ionic transport is more efficient for the FEG/MoO$_{3-x}$. In addition, the FEG/MoO$_{3-x}$ exhibits a much smaller diameter of the semi-circle and an equivalent series resistance (R_s, 0.82 ohm) compared to those of CC/MoO$_{3-x}$ (1.44 ohm, see the inset of Fig. 3a). This can be attributed to the contribution of 3D partially exfoliated graphite layers seamlessly connected with the bulky matrix, which leads to better conductivity within the electrode.

The electrode kinetics and charge storage mechanism were separated from diffusion-controlled and capacitive-controlled processes by Dunn's method (see ESI† for details).[24,25] The results for the FEG/MoO$_{3-x}$ and CC/MoO$_{3-x}$ electrodes are summarized at the selected scan rate of 1 mV s^{-1} in Fig. 3b and c. The FEG/MoO$_{3-x}$ electrode showed higher capacitive contribution (62.3%) than the CC/MoO$_{3-x}$ (29.3%). Fig. 3d compares the capacitive and diffusion contributions of the two electrodes at scan rates between 0.2 and 4 mV s^{-1}. It was found that the capacitive contribution of the FEG/MoO$_{3-x}$ was always higher than that of the CC/MoO$_{3-x}$ at all scan rates. Capacitive-controlled reactions typically have relatively fast kinetics compared to the diffusion-controlled processes by ion intercalation and de-intercalation in the oxide bulk structure.[26,27] Therefore, the more contribution from the capacitive-controlled capacitance, the more capacitance will be stored at ultrahigh current densities. This trend is in excellent agreement with our EIS results shown in Fig. 3a.

Overall, our results confirm the important roles of the three-dimensional porous graphene architecture and oxygen-containing functional groups for supporting a high mass loading of MoO$_{3-x}$. On the one hand, the engineered layered structure contains 3D intercalated graphite sheets interconnected with highly open graphene nanosheets atop. The multiple connection points create a "super highway" for a fast electron transportation pathway, while the large amount of void space allows sufficient electrolyte intercalation/de-intercalation into the electrode, thus providing rapid ionic transportation. On the other hand, the oxygen-containing functional groups ensure that the MoO$_{3-x}$ can bind strongly onto the exfoliated graphite *via* the formation of C–O–Mo bonding. This therefore facilitates the electron hopping process from the graphene to the oxide, and thus allows excellent rate performance with ultrahigh mass loading. In addition, the deposited MoO$_{3-x}$ is amorphous in nature featuring mixed-valence distribution, as demonstrated earlier, which can be beneficial to the charge

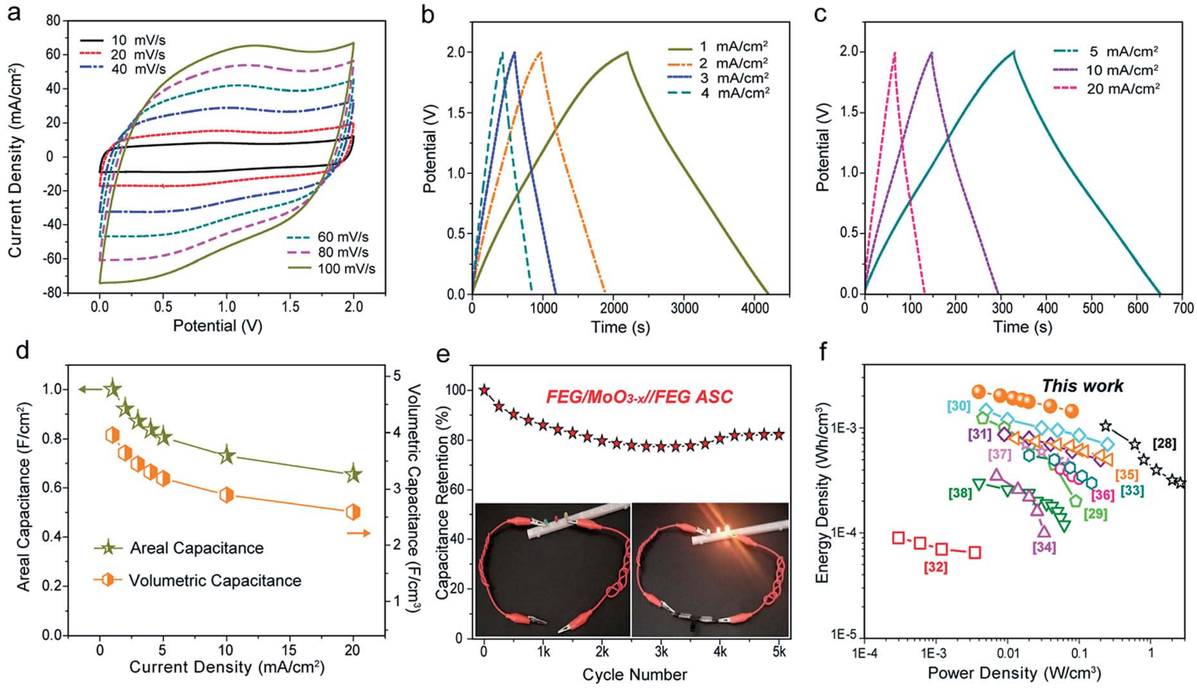

Fig. 4 (a) CV curves of the ASC device measured at different scan rates. (b and c) GCD profiles of the ASC device collected at various current densities. (d) Areal and volumetric capacitance of the ASC device measured at different current densities. (e) Cycling stability of the ASC device tested at a scan rate of 100 mV s^{-1}, the inset shows that the fully charged solitary ASC operates an LED lighting matrix. (f) Ragone plots of the ASC device with other reported ASCs.

storage process due to the flexibility and multiple redox reactions. As a whole, the novel composite electrode material designed here in this work shows a substantially increased mass loading of pseudocapacitive MoO_{3-x} without sacrificing the charge storage capability, which is essential for developing promising supercapacitors.

Asymmetric supercapacitors

A practical asymmetric supercapacitor (ASC) device was fabricated through the assembly of an FEG/MoO_{3-x} anode and a functionalized partially exfoliated graphite cathode (see the Experimental section and detailed electrochemical performance of the cathode in the ESI†). Fig. 4a shows the CV curves of the ASC device at different scan rates with a large operating voltage of 2 V. No significant distortion with the increase of scan rate was observed, suggesting the good rate capability of the ASC device. The GCD curves of the ASC devices collected at different current densities (1–20 mA cm^{-2}) are shown in Fig. 4b and c. The symmetric GCD profiles demonstrate an ideal capacitive behavior. The ASC exhibits excellent areal and volumetric capacitances of 1.0 F cm^{-2} and 3.96 F cm^{-3} at the current density of 1 mA cm^{-2}. More importantly, as the current density increases 20 times, the ASC device still retains an extraordinary rate capability of 65.6% from 1 to 20 mA cm^{-2} (Fig. 4d). The ASC retains 82.2% capacitance after 5000 CV cycles (Fig. 4e). Furthermore, two model devices connected in series can effectively operate green, red and yellow light-emitting diodes and an electrical fan at the fully charged voltage of 4 V, demonstrating its potential for practical applications (Fig. 4e inset and Fig. S19†). The energy and power densities of our FEG/MoO_{3-x}// FEG device are shown in the Ragone plot in Fig. 4f. The device displays a high volumetric energy density of 2.20 mW h cm^{-3} at the power density of 3.60 mW cm^{-3}, and 1.44 mW h cm^{-3} at the high power density of 79.1 mW cm^{-3}. It should be noted that these values are essentially greater than the values obtained for the other capacitor devices reported to date.[28–38] We also assembled an all-solid asymmetric supercapacitor with KCl/PVA as the electrolyte. Fig. S20a† shows the GCD curves of the all-solid ASC device at different current densities (1 mA cm^{-2} to 20 mA cm^{-2}). The all-solid ASC displays a high areal capacitance of 0.71 F cm^{-2} and a volumetric capacitance of 2.82 F cm^{-3} at 1 mA cm^{-2} (Fig. S20b and c†). We also tested the practical usage of the all-solid ASC. The charged device can also effectively operate green, red and yellow light-emitting diodes (LEDs). The all-solid ASC device displays high energy density and powder density as shown in the Ragone plot (Fig. S20f†), with a volumetric energy density of 1.57 mW h cm^{-3} obtained at the power density of 11.34 mW cm^{-3}.

Conclusions

In summary, an ultrahigh mass loading molybdenum oxide was electrodeposited on 3D functionalized partially exfoliated graphite with improved capacitance and rate capability. The engineered layered structure, combining intercalated graphite sheets and highly open graphene nanosheets atop, allowed efficient ion diffusion and thus enabled an ultrahigh mass loading of pseudocapacitive materials without sacrificing the electrochemical performance. The optimized electrode achieved an outstanding areal capacitance of 4.34 F cm^{-2} at 1 mA cm^{-2} and excellent rate capability. The ASC assembled with the FEG/MoO_{3-x} anode and FEG cathode delivered an excellent volumetric capacitance of 3.96 F cm^{-3} as well as a high volumetric energy density of 2.20 mW h cm^{-3}. More importantly, the linear increase of areal capacitance with the mass loading of MoO_{3-x} suggests its great potential for practically viable pseudocapacitors.

Conflicts of interest

There are no conflicts to declare.

Acknowledgements

This work was financially supported by the Liaoning Revitalization Talents Program – Pan Deng Scholars (XLYC1802005), the Liaoning BaiQianWan Talents Program, the National Science Fund of Liaoning Province for Excellent Young Scholars, the Science and Technology Innovative Talents Support Program of Shenyang (RC180166), the Australian Research Council (ARC) through the Discovery Early Career Researcher Award (DE150101306) and the Linkage Project (LP160100927), the Faculty of Science Strategic Investment Funding 2019 of University of Newcastle, and CSIRO Energy, Australia.

References

1 M. Yu, D. Lin, H. Feng, Y. Zeng, Y. Tong and X. Lu, *Angew. Chem., Int. Ed.*, 2017, **56**, 1–6.

2 Z. H. Huang, Y. Song and X. X. Liu, *Chem. Eng. J.*, 2019, **358**, 1529–1538.

3 Y. Zeng, Z. Lai, Y. Han, H. Zhang, S. Xie and X. Lu, *Adv. Mater.*, 2018, 1802396.

4 Z. H. Huang, Y. Song, X. X. Xu and X. X. Liu, *ACS Appl. Mater. Interfaces*, 2015, **7**, 25506–25513.

5 H. Ji, X. Liu, Z. Liu, B. Yan, L. Chen, Y. Xie, C. Liu, W. Hou and G. Yang, *Adv. Funct. Mater.*, 2015, **25**, 1886–1894.

6 L. Huang, B. Yao, J. Sun, X. Gao, J. Wu, T. Li, Z. Hu and J. Zhou, *J. Mater. Chem. A*, 2017, **5**, 2897–2903.

7 P. M. Shafi, R. Dhanabal, A. Chithambararaj, S. Velmathi and A. C. Bose, *ACS Sustainable Chem. Eng.*, 2017, **5**, 4757–4770.

8 Q.-L. Lu, S.-X. Zhao, C.-K. Chen, X. Wang, Y.-F. Deng and C.-W. Nan, *J. Mater. Chem. A*, 2016, **4**, 14560–14566.

9 W. Zeng, G. Zhang, S. Hou, T. Wang and H. Duan, *Electrochim. Acta*, 2015, **151**, 510–516.

10 K. Lu, B. Song, K. Li, J. Zhang and H. Ma, *J. Power Sources*, 2017, **370**, 98–105.

11 B. Yao, S. Chandrasekaran, J. Zhang, W. Xiao, F. Qian, C. Zhu, E. Duoss, C. Spadaccini, M. Worsley and Y. Li, *Joule*, 2019, **3**, 459–470.

12 M. D. Stoller and R. S. Ruoff, *Energy Environ. Sci.*, 2010, **3**, 1294–1301.

13 Z. H. Huang, Y. Song, D. Y. Feng, Z. Sun, X. Sun and X. X. Liu, *ACS Nano*, 2018, **12**, 3557–3567.

14 Y. Gogotsi and P. Simon, *Science*, 2011, **334**, 917–918.

15 K. Zhou, W. Zhou, Z. Liu, Y. Sang, S. Ji, W. Li, J. Lu, L. Li, W. Niu, H. Liu and S. Chen, *Nano Energy*, 2015, **12**, 510–520.

16 G. Zhou, D.-W. Wang, L.-C. Yin, N. Li, F. Li and H.-M. Cheng, *ACS Nano*, 2012, **6**, 3214–3223.

17 Y. Song, X. Cai, X. Xu and X.-X. Liu, *J. Mater. Chem. A*, 2015, **3**, 14712–14720.

18 H. B. Li, M. H. Yu, F. X. Wang, P. Liu, Y. Liang, J. Xiao, C. X. Wang, Y. X. Tong and G. W. Yang, *Nat. Commun.*, 2013, **4**, 1894.

19 J. Noh, C.-M. Yoon, Y. K. Kim and J. Jang, *Carbon*, 2017, **116**, 470–478.

20 C. Guan, X. Liu, W. Ren, X. Li, C. Cheng and J. Wang, *Adv. Energy Mater.*, 2017, **7**, 1602391.

21 Z. H. Huang, T. Y. Liu, Y. Song, Y. Li and X. X. Liu, *Nanoscale*, 2017, **9**, 13119–13127.

22 C. Zhu, S. Fu, D. Du and Y. Lin, *Chem.–Eur. J.*, 2016, **22**, 4000–4007.

23 Z.-H. Huang, F.-F. Sun, M. Batmunkh, W.-H. Li, H. Li, Y. Sun, Q. Zhao, X. Liu and T.-Y. Ma, *J. Mater. Chem. A*, 2019, **7**, 11826–11835.

24 V. Augustyn, P. Simon and B. Dunn, *Energy Environ. Sci.*, 2014, **7**, 1597–1614.

25 W. Yan, T. Ayvazian, J. Kim, Y. Liu, K. Donavan, W. Xing, Y. Yang, J. Hemminger and R. Penner, *ACS Nano*, 2011, **5**, 8275–8287.

26 J. Duay, S. Sherrill, Z. Gui, E. Gillette and S. B. Lee, *ACS Nano*, 2013, **7**, 1200–1214.

27 T. Zhai, X. Lu, Y. Ling, M. Yu, G. Wang, T. Liu, C. Liang, Y. Tong and Y. Li, *Adv. Mater.*, 2014, **26**, 5869–5875.

28 J. Chen, S. Han, H. Zhao, J. Bai, L. Wang, G. Sun, Z. Zhang, X. Pan, J. Zhou and E. Xie, *Chem. Eng. J.*, 2017, **320**, 34–42.

29 Z. Zhang, K. Chi, F. Xiao and S. Wang, *J. Mater. Chem. A*, 2015, **3**, 12828–12835.

30 G. Yilmaz, C. X. Guo and X. M. Lu, *ChemElectroChem*, 2016, **3**, 158–164.

31 Z. Zhang, F. Xiao and S. Wang, *J. Mater. Chem. A*, 2015, **3**, 11215–11223.

32 F. M. Wang, Y. C. Li, Z. Z. Cheng, K. Xu, X. Y. Zhan, Z. X. Wang and J. He, *Phys. Chem. Chem. Phys.*, 2014, **16**, 12214–12220.

33 P. H. Yang, Y. Ding, Z. Y. Lin, Z. W. Chen, Y. Z. Li, P. F. Qiang, M. Ebrahimi, W. J. Mai, C. P. Wong and Z. L. Wang, *Nano Lett.*, 2014, **14**, 731–736.

34 J. X. Feng, S. H. Ye, X. F. Lu, Y. X. Tong and G. R. Li, *ACS Appl. Mater. Interfaces*, 2015, **7**, 11444–11451.

35 D. Y. Feng, Y. Song, Z. H. Huang, X. X. Xu and X. X. Liu, *J. Power Sources*, 2016, **324**, 788–797.

36 X. H. Lu, Y. X. Zeng, M. H. Yu, T. Zhai, C. L. Liang, S. L. Xie, M. Balogun and Y. X. Tong, *Adv. Mater.*, 2014, **26**, 3148–3155.

37 T. Zhai, X. H. Lu, Y. C. Ling, M. H. Yu, G. M. Wang, T. Y. Liu, C. L. Liang, Y. X. Tong and Y. Li, *Adv. Mater.*, 2014, **26**, 5869–5875.

38 Q. Q. Tang, M. M. Chen, C. Y. Yang, W. Q. Wang, H. Bao and G. C. Wang, *ACS Appl. Mater. Interfaces*, 2015, **7**, 15303–15313.